



## Ductile Co–Nb–B bulk metallic glass with ultrahigh strength



Chaochao Dun<sup>a,b,c</sup>, Haishun Liu<sup>a,\*</sup>, Long Hou<sup>a</sup>, Lin Xue<sup>a,b,c</sup>, Lintao Dou<sup>a</sup>, Weiming Yang<sup>a,b,c</sup>, Yucheng Zhao<sup>a</sup>, Baolong Shen<sup>b,\*\*</sup>

<sup>a</sup> School of Sciences, State Key Laboratory for Geomechanics and Deep Underground Engineering, China University of Mining and Technology, Xuzhou 221116, China

<sup>b</sup> Materials Science and Engineering, Southeast University, Nanjing 211189, China

<sup>c</sup> Zhejiang Province Key Laboratory of Magnetic Materials and Application Technology, Key Laboratory of Magnetic Materials and Devices, Ningbo Institute of Materials Technology & Engineering, Chinese Academy of Sciences, Ningbo 315201, China

### ARTICLE INFO

#### Article history:

Received 28 September 2013

Received in revised form 10 November 2013

Available online 23 December 2013

#### Keywords:

Metallic glasses;

Strength;

Plasticity

### ABSTRACT

A ternary  $\text{Co}_{61}\text{Nb}_8\text{B}_{31}$  bulk metallic glass with plasticity of 5% and yield strength of 5200 MPa was fabricated. It is shown that the primary crystallization product of the  $\text{Co}_{61}\text{Nb}_8\text{B}_{31}$  glass is the vertex- and edge-sharing  $\text{Co}_2\text{Nb}$  type phase. The enhanced plastic strain is consistent with the observed multiple shear bands that can redistribute the internal shear stress. The appreciable plastic strain favors the formation of metallic bonding network-like structure and holds high Poisson's ratio.

© 2013 Elsevier B.V. All rights reserved.

### 1. Introduction

Bulk metallic glasses (BMGs) have attracted much attention not only because of their superior chemical [1], physical [2,3], magnetic properties [4,5], but also because of their excellent mechanical properties [6]. For a long time, the improvement in strength and plasticity of BMGs is a key topic in the development of advanced structure materials [7–9]. Compared with other BMGs, Co-based BMGs are very promising due to their ultrahigh strength, better resistance to corrosion and oxidation [10–13]. Especially,  $\text{Co}_{43}\text{Fe}_{20}\text{Ta}_{5.5}\text{B}_{31.5}$  [10,14] and  $\text{Co}_{65-x}\text{Ta}_x\text{B}_{35}$  (at. %,  $x = 5-11$ ) [11,15] systems have rapidly been of broad interest, which set the record for the highest strength among the known bulk glassy alloys. However, these alloys contain 5–11 at.% Ta element that has extremely high melting point, which makes these alloys brittle and extremely difficult to treat [11]. Since these great drawbacks of Co–(Fe)–Ta–B alloys for industrial applications, it is necessary to obtain the ductile Co-based MGs without Ta.

Poisson's ratio is proven to be one of important factors in guiding glassy alloy design to alleviate brittleness. A higher Poisson's ratio is beneficial to plasticity of metallic glasses [16]. In this paper, we utilized the possibility of tuning the Co–Ta–B alloy composition by replacing Ta by Nb to help designing a new ternary Co-based metallic glass with adequate plasticity. Here, Nb element is preferentially chosen based on three considerations: The first is Nb has the lower melting point than Ta. The second is the Nb with the highest Poisson's ratio in metal [17]. The third is Nb can stabilize the super-cooled liquid and possibly form the Co-based bulk MGs [18]. In view of these criteria, a new ternary

$\text{Co}_{61}\text{Nb}_8\text{B}_{31}$  BMG with significant plastic deformation about 5% at high strength value of 5200 MPa was obtained, which offers an opportunity to study thoroughly the deformation mechanisms of BMGs based on simplicity of its constituent elements. The high strength together with the promising plasticity is encouraging for further development of Co-based BMGs with potential applications.

### 2. Experiment

Alloy ingots with nominal compositions of  $\text{Co}_{61}\text{Nb}_8\text{B}_{31}$  were prepared by induction melting of pure elements (Co, Nb, B, 99.99%) under an argon atmosphere, followed by direct casting into cylindrical rods with 30 mm in length and 1 mm, 1.5 mm and 2 mm in diameter ( $\Phi$ ), respectively. Corresponding structures were characterized by X-ray diffraction (XRD) with monochromatic  $\text{Cu } K_{\alpha}$  radiation. Thermal properties were measured using differential scanning calorimeters (DSC). Density of sample was determined based on Archimedes' principle. The mechanical behaviors of at least 20 as-cast samples with diameter of 1 mm and aspect ratio of 2:1 were tested under uniaxial compression using Instron testing machine. The lateral and fracture surface morphologies were studied by scanning electron microscopy (SEM). In addition, thin slices from the as-cast rods were prepared by conventional method of slicing and grinding, followed by dimpling and finally ion-milling. These slices were subsequently used for detailed structural investigations by high resolution transmission electron microscopy (HRTEM).

### 3. Results and discussion

Fig. 1 shows a typical compressive strain–stress curve for the  $\text{Co}_{61}\text{Nb}_8\text{B}_{31}$  rod with 1 mm in diameter. The stress–strain curve shows

\* Corresponding author. Tel.: +86 139 12006872; fax: +86 516 83591591.

\*\* Corresponding author. Tel.: +86 574 8791 3392; fax: +86 574 8761 7212.

E-mail addresses: [liuhaishun@126.com](mailto:liuhaishun@126.com) (H. Liu), [blshen@seu.edu.cn](mailto:blshen@seu.edu.cn) (B. Shen).

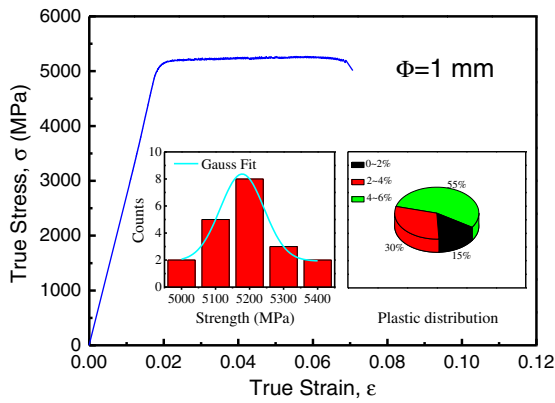


Fig. 1. Compressive stress–strain curve of  $\text{Co}_{61}\text{Nb}_8\text{B}_{31}$  glassy rod at room temperature. The insets are the experimental data distributions of strength and plasticity.

pronounced plastic flow and thus the yield strength ( $\sigma_y$ ) and compressive strength ( $\sigma_c$ ) can be precisely determined as 5200 MPa and 5290 MPa, respectively. On the other hand, the  $\text{Co}_{61}\text{Nb}_8\text{B}_{31}$  glassy rod also exhibits compressive plasticity of about 5%, which is much larger than plastic strain ( $\epsilon_p$ ) reported for other Co-based BMGs and most of other BMGs. Some mechanical properties of typical BMGs with high strength are summarized in Table 1. These results reveal that  $\text{Co}_{61}\text{Nb}_8\text{B}_{31}$  glassy rods possess both significant plastic deformation about 5% and superhigh compressive strength value 5200 MPa at the same time, which is rarely observed in other BMGs up to now. This superhigh strength and respectable plasticity of the present Co-based BMG are encouraging for developing high performance BMGs as structural materials.

Fig. 2 shows the XRD patterns and DSC trace obtained from  $\text{Co}_{61}\text{Nb}_8\text{B}_{31}$  BMG. The glass transition and crystallization behavior were measured at a continuous heating rate of 0.67 K/s, while the solidification behavior was measured at a cooling rate of 0.067 K/s. XRD pattern of  $\text{Co}_{61}\text{Nb}_8\text{B}_{31}$  rod ( $\Phi = 1.5$  mm) displays only a typical broad diffraction maxima without any detectable crystalline reflection, and DSC exhibits one endothermic event that is characteristic of glass transition from amorphous alloys into super-cooled liquid. These are characteristics of fully amorphous structure. We have also checked the XRD pattern of  $\text{Co}_{61}\text{Nb}_8\text{B}_{31}$  rod ( $\Phi = 2$  mm). Note that the primary crystallization product of the  $\text{Co}_{61}\text{Nb}_8\text{B}_{31}$  glass alloy is the vertex- and edge-sharing  $\text{Co}_2\text{Nb}$  type phase [19], instead of the covalent face-centered cubic  $\text{Co}_{21}\text{Ta}_2\text{B}_6$  bonds as observed in  $\text{Co}_{43}\text{Fe}_{20}\text{Ta}_{5.5}\text{B}_{31.5}$  [10].

Fig. 3 (a)–(c) shows the SEM images of the surface of the  $\text{Co}_{61}\text{Nb}_8\text{B}_{31}$  specimen after compression loading prior to failure. Localized main shear band appears in a near-elliptical morphology and ends up at the same side, which is characterized by a shear angle of about  $43.5^\circ$  to the compressive axis [see Fig. 3 (a)]. As can be seen in Fig. 3 (b), around the existing primary shear band, it is noted that several remarkable cracks and scattered shear bands are present. The formation of

Table 1

Mechanical properties ( $\sigma_y$ , yield strength;  $\sigma_c$ , compressive strength;  $\epsilon_p$ , plastic strain) of the present and some other typical BMGs with high yield strength, where  $\Phi$  is the measured diameter used in compression test at room temperature.

Glassy alloys	$\Phi$ (mm)	$\sigma_y$ (GPa)	$\sigma_c$ (GPa)	$\epsilon_p$ (%)	References
$\text{Co}_{61}\text{Nb}_8\text{B}_{31}$	1.0	5.2	5.29	5.0	This work
$\text{Co}_{59}\text{Ta}_6\text{B}_{35}$	1.0	5.41	5.72	1.5	[11]
$\text{Co}_{57}\text{Ta}_8\text{B}_{35}$	1.0	5.51	5.87	0.9	[11]
$\text{Co}_{43}\text{Fe}_{20}\text{Ta}_{5.5}\text{B}_{31.5}$	2.0	–	5.0	0	[10]
$(\text{Co}_{0.535}\text{Fe}_{0.1}\text{Ta}_{0.055}\text{B}_{0.31})_{98}\text{Mo}_2$	1.5	–	5.55	0	[14]
$[(\text{Co}_{0.535}\text{Fe}_{0.1}\text{Ta}_{0.055}\text{B}_{0.31})_{0.98}\text{Mo}_{0.02}]_{98}\text{Si}_2$	3.0	–	4.45	0	[14]
$(\text{Co}_{0.6}\text{Fe}_{0.4})_{68}\text{B}_{21.9}\text{Si}_{5.1}\text{Nb}_5$	5.0	–	4.38	1.0	[12]
$(\text{Co}_{0.7}\text{Fe}_{0.3})_{68}\text{B}_{21.9}\text{Si}_{5.1}\text{Nb}_5$	5.5	–	4.34	0.8	[12]

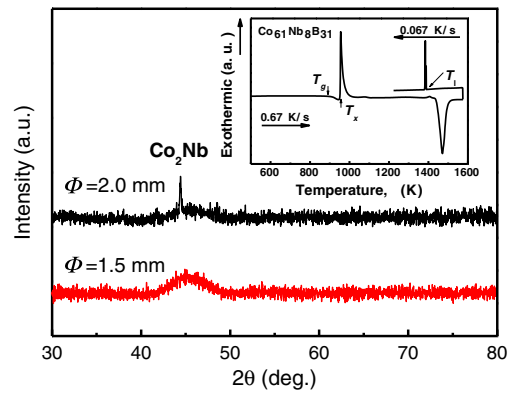


Fig. 2. XRD patterns of  $\text{Co}_{61}\text{Nb}_8\text{B}_{31}$  BMG with diameter of 1.5 mm and 2 mm. The inset is the DSC trace of  $\text{Co}_{61}\text{Nb}_8\text{B}_{31}$  BMG with diameter of 1 mm.

such cracks without instable propagation gives us a hint that the  $\text{Co}_{61}\text{Nb}_8\text{B}_{31}$  BMG holds a definite resistance to catastrophic failures of brittle materials. The enlarged region exhibits an obvious shear-

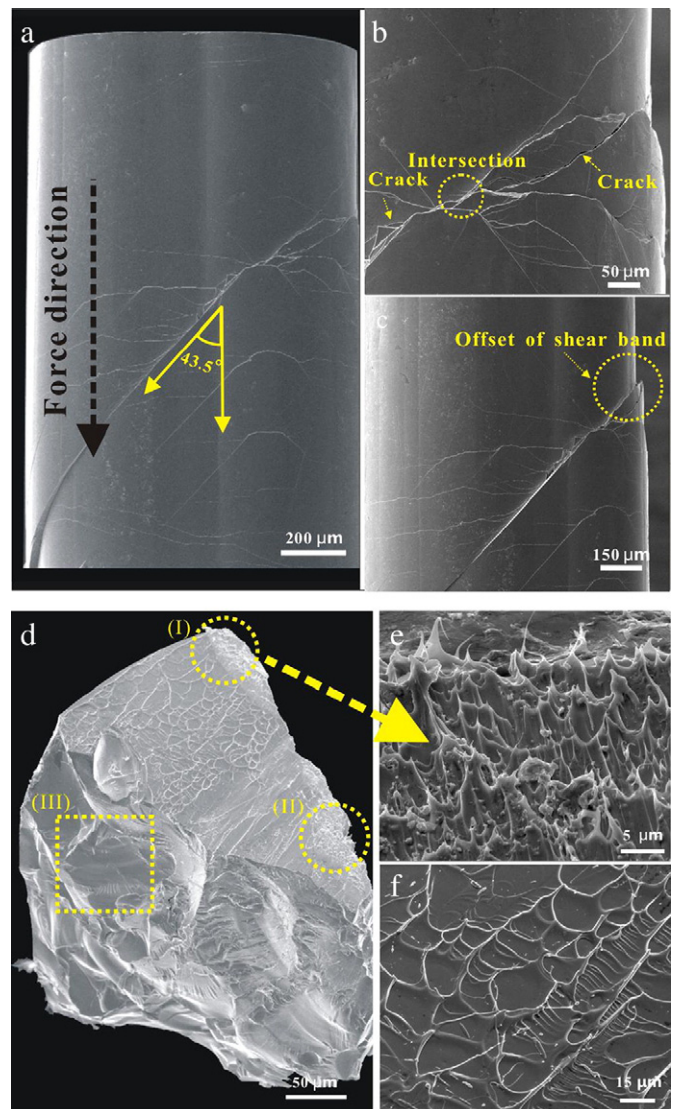
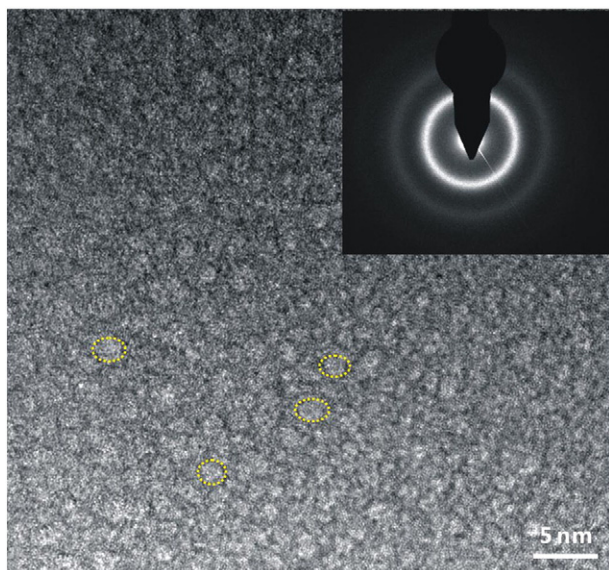


Fig. 3. SEM images of  $\text{Co}_{61}\text{Nb}_8\text{B}_{31}$  glassy rod, lateral view of the deformed specimen (a), the intersection and cracks (b), offset of shear band (c), fractographies after compressive fracture (d), melted liquid flow (e), and vein-like patterns (f).



**Fig. 4.** HRTEM image of  $\text{Co}_{61}\text{Nb}_8\text{B}_{31}$  glassy rod with diameter of 1 mm inset with SAED pattern.

deformation-induced slip in the compressive sample [see Fig. 3 (c)]. We further examine the fracture surfaces of  $\text{Co}_{61}\text{Nb}_8\text{B}_{31}$ , as shown in Fig. 3 (d)–(f). Fig. 3 (d) displays ductile fracture behavior of  $\text{Co}_{61}\text{Nb}_8\text{B}_{31}$  rod containing mixed features of vein-like patterns, melted liquid flow (Parts I and II), and the cleavage-like structures (Part III). The enlarged image of Part I is shown in Fig. 3 (e), which reveals details of the melted liquid flow on the fracture surface, indicating the occurrence of melting behavior caused by remarkable temperature rise due to the high elastic energy [20]. The flow-like structure is normally regarded as the solidification form of melted liquid flow if the cooling process is fast enough, as shown in Fig. 3 (f). The appearance of vein patterns and the protrusive shear offset related to the shear band movement can evidently verify the enhanced ductility of  $\text{Co}_{61}\text{Nb}_8\text{B}_{31}$ .

In MGs, the fundamental building blocks are solute-centered clusters, rather than individual atoms [21,22]. Some of these clusters are tightly connected, as they share atoms to form the medium short range (MRO) clusters [23,24]. This agrees with  $\text{Co}_{43}\text{Fe}_{20}\text{Ta}_{5.5}\text{B}_{31.5}$ , which has been identified by X-ray absorption fine structure measurement and *ab* initial molecular dynamics simulations [25]. Therefore, although no synchrotron or MD simulation data on MRO clusters have been obtained for the  $\text{Co}_{61}\text{Nb}_8\text{B}_{31}$  glassy alloy, the similarities of structure and alloy components allow us to posit the formation of the MRO clusters. The HRTEM image and inserted selected area electronic diffraction (SAED) pattern of the investigated samples show certain evidence for the formation of MRO clusters in the  $\text{Co}_{61}\text{Nb}_8\text{B}_{31}$  glassy matrix, as shown in Fig. 4. The initial nucleation of shear bands might be related to plastic instabilities in some local order regions. The physical nature of the formation of MRO is caused by the strong bonding tendency that acts as the origin of the ultrahigh resistance against fracture and plastic yielding [17]. The atomic bonds within clusters are stronger while the atomic interactions linking the clusters and super-clusters are weaker. The crack initiation and propagation normally occur firstly between the clusters [26,27]. Among clusters in contact, shear is more readily accommodated by vertex- and edge-sharing clusters than by face-sharing clusters [28]. Thus, during compression for  $\text{Co}_{61}\text{Nb}_8\text{B}_{31}$ ,

the stress mismatch resulting from the MRO can lead to the initiation of shear bands, which would result in an increasing number of shear bands arising during deformation. Furthermore, such MRO may indirectly hamper shear band propagation and make them tend to bifurcate and branch. They can also increase the resistance to flow deformation by increasing the viscosity inside the shear bands. Therefore, the  $\text{Co}_{61}\text{Nb}_8\text{B}_{31}$  BMG with large plasticity.

#### 4. Conclusions

In conclusion, a ternary  $\text{Co}_{61}\text{Nb}_8\text{B}_{31}$  BMG with appreciable compressive plasticity of 5%, combined with high yield strength of 5200 MPa was fabricated. The multiple shear bands, vein-like patterns as well as the melted liquid flow were observed on the fracture surface. The microstructure of the metallic glass exhibits random network-like MRO clusters, which have the ability to promote plasticity by activating easy nucleation and continuous multiple shear bands throughout the whole metallic glass. This alloy is a promising model material for studying the structural and functional properties of BMGs.

#### Acknowledgments

We appreciate the editor and reviewer's constructive suggestion and valuable advice. This work was supported by the National Natural Science Foundation of China (Grant Nos. 51074155, 50825103, 51271194, and 50834004), and National Basic Research Program of China (2010CB226805).

#### References

- [1] J.-Q. Wang, Y.-H. Liu, M.-W. Chen, G.-Q. Xie, D.V. Louzguine-Luzgin, A. Inoue, J.H. Perepezko, *Adv. Funct. Mater.* 22 (2012) 2567–2570.
- [2] W. Yang, H. Liu, C. Dun, J. Li, Y. Zhao, B. Shen, *J. Non-Cryst. Solids* 361 (2013) 82–85.
- [3] W.H. Wang, C. Dong, C.H. Shek, *Mater. Sci. Eng. R* 44 (2004) 45–89.
- [4] W. Yang, H. Liu, L. Xue, J. Li, C. Dun, J. Zhang, Y. Zhao, B. Shen, *J. Magn. Mater.* 335 (2013) 172–176.
- [5] A. Inoue, B.L. Shen, H. Koshiba, H. Kato, A.R. Yavari, *Acta Mater.* 52 (2004) 1631–1637.
- [6] A. Inoue, B.L. Shen, A. Takeuchi, *Mater. Sci. Eng. A* 441 (2006) 18–25.
- [7] K.F. Yao, F. Ruan, Y.Q. Yang, N. Chen, *Appl. Phys. Lett.* 88 (2006) 122106.
- [8] T. Zhang, F. Liu, S. Pang, R. Li, *Mater. Trans.* 48 (2007) 1157–1160.
- [9] J.M. Park, G. Wang, R. Li, N. Mattern, J. Eckert, D.H. Kim, *Appl. Phys. Lett.* 96 (2010) 031905.
- [10] A. Inoue, B. Shen, H. Koshiba, H. Kato, A.R. Yavari, *Nat. Mater.* 2 (2003) 661–663.
- [11] J.F. Wang, R. Li, N.B. Hua, T. Zhang, *J. Mater. Res.* 26 (2011) 2072–2079.
- [12] Y. Dong, Q. Man, H. Sun, B. Shen, S. Pang, T. Zhang, A. Makino, A. Inoue, *J. Alloys Compd.* 509 (2011) S206–S209.
- [13] J.T. Fan, Z.F. Zhang, B.L. Shen, S.X. Mao, *Scr. Mater.* 59 (2008) 603–606.
- [14] B.L. Shen, A. Inoue, *J. Phys. Condens. Matter* 17 (2005) 5647–5653.
- [15] J.F. Wang, R. Li, R.J. Xiao, T. Xu, Y. Li, Z.Q. Liu, L. Huang, N.B. Hua, G. Li, Y.C. Li, T. Zhang, *Appl. Phys. Lett.* 99 (2011).
- [16] Y.H. Liu, G. Wang, R.J. Wang, Q. Zhao de, M.X. Pan, W.H. Wang, *Science* 315 (2007) 1385–1388.
- [17] J.H. Yao, J.Q. Wang, Y. Li, *Appl. Phys. Lett.* 92 (2008) 251906.
- [18] H.J. Sun, Q.K. Man, Y.Q. Dong, B.L. Shen, H. Kimura, A. Makino, A. Inoue, *J. Alloys Compd.* 504 (2010) S31–S33.
- [19] A. Inoue, *Acta Mater.* 48 (2000) 279–306.
- [20] J.J. Lewandowski, A.L. Greer, *Nat. Mater.* 5 (2006) 15–18.
- [21] D.B. Miracle, *Nat. Mater.* 3 (2004) 697–702.
- [22] A. Hirata, P. Guan, T. Fujita, Y. Hirotsu, A. Inoue, A.R. Yavari, T. Sakurai, M. Chen, *Nat. Mater.* 10 (2011) 28–33.
- [23] H.W. Sheng, W.K. Luo, F.M. Alamgir, J.M. Bai, E. Ma, *Nature* 439 (2006) 419–425.
- [24] D. Ma, A.D. Stoica, X.L. Wang, *Nat. Mater.* 8 (2009) 30–34.
- [25] X. Hui, D.Y. Lin, X.H. Chen, W.Y. Wang, Y. Wang, S.L. Shang, Z.K. Liu, *Scr. Mater.* 68 (2013) 257–260.
- [26] E.S. Park, H.J. Chang, D.H. Kim, *Acta Mater.* 56 (2008) 3120–3131.
- [27] W.H. Wang, *J. Appl. Phys.* 111 (2012) 123519.
- [28] C. Jiang, S.G. Srinivasan, A. Caro, S.A. Maloy, *J. Appl. Phys.* 103 (2008).